Available online at www.sciencedirect.com
ScienceDirect
Journal of Solid State Chemistry 180 (2007) 907–914
JOURNAL OF SOLID STATE CHEMISTRY
www.elsevier.com/locate/jssc

Growth of new ternary intermetallic phases from Ca/Zn eutectic flux

Milorad Stojanovic, Susan E. Latturner*

Department of Chemistry and Biochemistry, Florida State University, Tallahassee, FL 32306-4390, USA

Received 10 August 2006; received in revised form 26 October 2006; accepted 14 December 2006
Available online 30 December 2006

Abstract

The eutectic 7.3:2.7 molar ratio mixture of calcium and zinc metal melts at 394 °C and was explored as a solvent for the growth of new intermetallic phases for potential use as hydrogen storage materials. The reaction of nickel in this molten mixture produces two new phases—the $CaCu_5$-related structure $CaNi_2Zn_3$ (*P6/mmm*, $a = 8.9814(5)$ Å, $c = 4.0665(5)$ Å) and a new cubic structure $Ca_{21}Ni_2Zn_{36}$ (*Fd–3m*, $a = 21.5051(4)$ Å). Palladium-containing reactions produced $CaPd_{0.85}Zn_{1.15}$ with the orthorhombic TiNiSi structure type (*Pnma*, $a = 7.1728(9)$ Å, $b = 4.3949(5)$ Å, $c = 7.7430(9)$ Å). Reactions of platinum in the Ca/Zn mixture produce $Ca_6Pt_3Zn_5$, with an orthorhombic structure related to that of W_3CoB_3 (*Pmmn*, $a = 13.7339(9)$ Å, $b = 4.3907(3)$ Å, $c = 10.7894(7)$ Å).

Keywords: Flux; Calcium; Zinc; Eutectic; Intermetallic; Crystal; Nickel; Palladium; Platinum; Hydrogen storage

1. Introduction

A number of investigations have shown molten metal fluxes to be a powerful tool in materials synthesis [1,2]. The solubility of many reactants in molten metal renders them active at temperatures well below their melting point. Lower temperatures and the modified energetics in a flux allow for the isolation of complex metastable or kinetically stabilized phases, instead of the thermodynamic sinks (such as simple binary phases with highly stable structures) favored by high-temperature reactions. In contrast to the powders often obtained by conventional solid-state synthesis methods, the solution phase character of flux reactions promotes the growth of crystals, which are required for accurate structural and electronic characterization. A wide variety of metals have been used as solvents, with Sn, Ga, Al, and In being most common. Calcium has not been investigated as a flux due to its high melting point, volatility at high temperatures, and reactivity toward common crucible materials. We have found that the formation of a eutectic with zinc permits the use of calcium-rich solvents for intermetallic synthesis at temperatures that minimize its volatility and reactivity toward reaction vessels.

Intermetallic compounds have come to the forefront as hydrogen storage materials due to their combination of high hydrogen capacity, close-to-ambient pressures and temperatures needed for activation, and the reversibility of the hydriding process [3]. These intermetallics are comprised of a very electropositive hydride-forming metal A (an element that will combine with H_2 to form a stable hydride, such as CaH_2) and a non-hydride forming metal B (a more electronegative transition metal that does not form a stable hydride). When these element classes are combined into an intermetallic phase, the resulting compound is often able to reversibly absorb hydrogen [4].

While $LaNi_5$ and other phases such as $ZrMn_2$ and YFe_3 have good hydrogen absorption kinetics, their high density is problematic. Investigations are needed to find other compounds with suitable absorption behavior that are comprised of lighter elements, and exploratory synthesis in flux mixtures is a promising avenue to investigate. Calcium and zinc are both relatively light metals; addition of an electronegative transition metal to a molten Ca/Zn eutectic mixture may result in formation of new intermetallic phases amenable to hydrogen absorption. Reactions of

*Corresponding author. Fax: +850 644 8281.
E-mail addresses: stojanovic@chem.fsu.edu (M. Stojanovic), latturne@chem.fsu.edu (S.E. Latturner).

0022-4596/$ - see front matter © 2007 Elsevier Inc. All rights reserved.
doi:10.1016/j.jssc.2006.12.022

group 10 metals (Ni, Pd, Pt) in this eutectic has produced the new phases $CaNi_2Zn_3$, $Ca_{21}Ni_2Zn_{36}$, $CaPd_{0.85}Zn_{1.15}$, and $Ca_6Pt_3Zn_5$.

2. Experimental procedure

2.1. Synthesis

Reactants were used as received: Ca shot (99.5%, Alfa Aesar), Zn granules (99.8%, Alfa Aesar), Ni powder (99.9%, Strem Chemicals), Pt powder (99.9%, Alfa Aesar), and Pd powder (99.9%, Strem Chemicals). The initial reactant ratio was a 6:2:1 mmole ratio of Ca/Zn/(Ni, Pd, or Pt) elements. The reactants were placed into stainless-steel crucibles (5.8 cm length/0.9 cm diameter), with the calcium loaded last to allow it to melt and flow over the other reactants. The crucibles were then sealed into a fused silica tube under vacuum. The reaction was heated to 900 °C in 6 h and was kept at this temperature for 12 h. Thereafter, the reaction was slowly cooled to 750 °C in 32 h, kept at 750 °C for 36 h, cooled to 600 °C in 36 h, kept at 600 °C for 12 h and cooled to room temperature in 48 h. After the cooling was finished, the crucible containing the reaction mixture was placed in water and sonicated for an hour to dissolve the excess calcium-rich flux. The remaining product was washed with water and acetone and left to dry overnight. Gray powder and shiny gold-tinged metallic crystals were obtained. Occasionally, the crystals were coated with excess flux and they appeared gray. Representative yields of such reactions are 150 mg $Ca_{21}Ni_2Zn_{36}$ and 60 mg of $CaNi_2Zn_3$ from reactions of 6:2:1 mmoles of Ca/Zn/Ni; 160 mg of $CaPd_{0.85}Zn_{1.15}$ from the Ca/Zn/Pd reaction, and 280 mg of $Ca_6Pt_3Zn_5$ from the Ca/Zn/Pt reaction.

Attempts to change the reactant ratio or scale up the reaction did not increase the yield. The ratios of 9:3:1.5 and 12:4:2, respectively, were set up but the amount of product did not increase. Instead, more gray powder was obtained, and an increased attack on the quartz tubes was observed. The tubes are darkened and discolored after the normal scale reactions; if the amount of Ca is too high, the tubes will fail due to the increased amount of calcium vapor pressure. Isolation of the products by centrifugation was tried for the Ca/Ni/Zn system; the reaction was prepared in an identical way, but an iron screen (100 mesh) was placed on top of the loaded crucible and held in place by an empty crucible on top of it. The fused silica tube was then sealed under vacuum and heated using a program similar to the one described above. However, after the temperature was cooled to 600 °C, it was held at this temperature for 48 h, then cooled to 450 °C in 48 h. At this temperature, the tube was removed from the furnace, inverted, and centrifuged to force the excess molten Ca/Zn eutectic through the iron screen. The crystals isolated in the reaction crucible were slightly larger than those recovered through etching off the solidified flux.

Stoichiometric syntheses were also attempted by combining the elements in the ratios found in the flux-grown crystalline products. Stainless-steel crucibles were used, with a solid steel ingot on top to limit volatilization of reactants; the heating profile was the same as that used for flux growth. The products were powders; they were mixed with silicon as an internal standard and were analyzed by powder X-ray diffraction. Only the CaPdZn phase was able to be obtained from a stoichiometric reaction (vide infra). The rest of the reactions yielded binary phases, predominantly $CaZn_2$ and $CaZn_3$.

2.2. Elemental analysis

Samples from each reaction were affixed to an aluminum SEM stub using carbon tape. Elemental analysis was performed on all samples using a JEOL 5900 scanning electron microscope with energy-dispersive X-ray spectroscopy (EDXS) capabilities. Samples were analyzed using a 30 kV accelerating voltage and an accumulation time of 60 s. The EDXS analysis was fairly inconsistent and it depended on the amount of flux coating the crystals. Better results were obtained by cleaving the crystals and analyzing the inner surface. Representative Ca/X/Zn ratios of 35:5:60 (for $Ca_{21}Ni_2Zn_{36}$), 20:30:50 ($CaNi_2Zn_3$), 35:30:35 ($CaPd_{0.85}Zn_{1.15}$), and 45:15:40 ($Ca_6Pt_3Zn_5$) were observed.

2.3. X-ray diffraction

Single-crystal X-ray diffraction data was collected at room temperature using a Bruker AXS SMART CCD diffractometer with a Mo radiation source. Processing of the data was accomplished with use of the program SAINT; an absorption correction was applied to the data using the SADABS program. Refinement of the structure was performed using the SHELXTL package [5]. For the two Ca/Ni/Zn phases, nickel and zinc sites were difficult to distinguish in the X-ray data due to their similar electron density; non-calcium sites were initially refined as zinc and then nickel sites were assigned based on bond length arguments, comparison to other structures reported in the literature, and elemental analysis. Surprisingly, the *R*-values in both refinements did go down slightly when the Ni sites were assigned. In the final refinement cycle, the occupancies of Ni and Zn sites were allowed to vary to determine if mixed occupancy was present. The occupancies ranged from 0.98 to 1.01, but this does not rule out mixed occupancy (vide infra). Crystallographic parameters and atom position data for all four phases can be found in Tables 1–6. STRUCTURE TIDY was used to standardize the atomic coordinates [6]. Additional details regarding the crystallographic refinements can be obtained from the Fachsinformationszentrum Karlsruhe, 76344 Eggenstein-Leopoldshafen, Germany (e-mail: www.crysdata@fiz.karlsruhe.de) on quoting the depository numbers 417124

Table 1
Crystallographic data collection parameters for Ca/X/Zn intermetallic phases

Compound	$CaNi_2Zn_3$	$Ca_{21}Ni_2Zn_{36}$	$CaPd_{0.85}Zn_{1.15}$	$Ca_6Pt_{2.33}Zn_{5.67}$
Formula weight	353.61	3312.42	204.94	1067.06
Space group	*P6/mmm*	*Fd–3m*	*Pnma*	*Pmmn*
a (Å)	8.9814(5)	21.5051(4)	7.1728(9)	4.3907(3)
b (Å)			4.3949(5)	13.7339(9)
c (Å)	4.0665(5)		7.7430(9)	10.7894(7)
V (Å^3)	284.08(4)	9945.4(3)	244.09(5)	650.62(4)
δ_{calc} (g/cm^3)	6.20	4.42	5.58	5.88
Z	3	8	4	2
Temperature (K)		298		
Radiation		Mo*K*α		
Index ranges	$-11\le h,k\le 11$	$-28\le h,k,l\le 28$	$-9\le h\le 9$	$-5\le h\le 5$
	$-5\le l\le 5$		$-5\le k\le 5$	$-18\le k\le 18$
			$-10\le l\le 10$	$-14\le l\le 14$
Absorption coeff. (mm^{-1})	29.6	19.9	19.1	43.5
Reflections collected	3844	32974	3056	8905
Unique data/parameters	172/20	638/38	342/21	950/50
R_1/wR_2 (all data)*	0.0246/0.0576	0.0494/0.0879	0.0274/0.0673	0.0320/0.0657
Residual peak/hole (e$^-$ Å^{-3})	0.954/−0.887	1.236/−1.865	1.43/−0.68	1.822/−2.483

*$R_1 = \Sigma\|F_o| - |F_c\|/\Sigma|F_o|$; $wR_2 = [\Sigma[w(F_o^2 - F_c^2)^2]/\Sigma[w(F_o^2)^2]]^{1/2}$.

Table 2
Atomic positions for $CaNi_2Zn_3$

Atom	Wyckoff site	*x*	*y*	*z*	U_{eq}
Ca1	1*b*	0	0	1/2	0.0067(8)
Ca2	2*c*	1/3	2/3	0	0.0066(6)
Ni1	6*m*	0.1820(1)	0.3640(2)	1/2	0.0053(3)
Zn1	3*g*	1/2	0	1/2	0.0066(4)
Zn2	6*j*	0.2928(1)	0	0	0.0064(3)

U_{eq} is defined as one-third of the trace of the orthogonalized U_{ij} tensor.

Table 3
Atomic positions for $Ca_{21}Ni_2Zn_{36}$

Atom	Wyckoff site	*x*	*y*	*z*	U_{eq}
Ca1	96*g*	0.06858(7)	0.06858(7)	0.3708(1)	0.0087(4)
Ca2	32*e*	0.2165(1)	0.2165(1)	0.2165(1)	0.0066(7)
Ca3	8*a*	1/8	1/8	1/8	0.005(1)
Ca4	32*e*	0.4438(1)	0.4438(1)	0.4438(1)	0.0143(9)
Ni1	16*c*	0	0	0	0.0049(7)
Zn1	96*g*	0.28569(4)	0.28569(4)	0.10944(6)	0.0081(3)
Zn2	96*g*	0.33332(4)	0.33332(4)	0.00711(6)	0.0083(3)
Zn3	96*g*	0.32035(5)	0.32035(5)	0.22513(6)	0.0113(3)

U_{eq} is defined as one third of the trace of the orthogonalized U_{ij} tensor.

Table 4
Selected bond lengths (in Å) in $CaNi_2Zn_3$ and $Ca_{21}Ni_2Zn_{36}$

$CaNi_2Zn_3$		$Ca_{21}Ni_2Zn_{36}$	
Ni–Zn1	2.4821(5) × 2	Ni–Zn1	2.592(1) × 6
Ni–Zn2	2.4839(3) × 4	Ni–Zn2	2.539(1) × 6
Ca1–Ni	2.831(1) × 6	Ca–Zn range	3.111(1)–3.315(2)
Ca2–Ni	3.1107(9) × 6	Ca–Ca1, Ca2, or Ca3 range	3.406(4)–3.486(4)
Ca1–Zn2	3.3245(8) × 6	Ca–Ca4 range	4.006(3)–4.185(4)
Ca2–Zn2	3.1912(6) × 6	Zn–Zn intericosahedral	2.635(2)–2.750(2)
Zn1–Zn2	2.7560(7) × 3	Zn2–Zn2 intraicosahedral	2.535(3)
Zn2–Zn2	2.630(1) × 2	Zn3–Zn3 triangles	2.896(2)
		Zn1–Zn3	2.702(2)

Table 5
Atomic positions for $CaPd_{0.85}Zn_{1.15}$

Atom	Wyckoff site	*x*	*y*	*z*	Occ.	U_{eq}
Ca	4*c*	0.0115(2)	1/4	0.6913(2)	1	0.0149(6)
Pd1/Zn1	4*c*	0.2927(1)	1/4	0.3975(1)	0.85(3)/0.15(3)	0.0152(3)
Zn2	4*c*	0.1654(2)	1/4	0.0766(1)	1	0.0167(4)

U_{eq} is defined as one third of the trace of the orthogonalized U_{ij} tensor.

($Ca_6Pt_3Zn_5$), 417125 ($CaPd_{0.85}Zn_{1.15}$), 417126 ($CaNi_2Zn_3$), and 417127 ($Ca_{21}Ni_2Zn_{36}$).

Powder X-ray diffraction data was collected for the products of the stoichiometric reactions, as well as powdered products found in the flux reactions. Samples were analyzed using a Rigaku Ultima III powder diffractometer. The MDI JADE 7.0 X-ray pattern data processing software was used to determine which phases were present and to calculate cell parameters.

3. Results and discussion

A series of reactions were prepared in a 73% calcium/27% zinc eutectic mixture that melts at 394 °C [7]. This enabled much of the reaction heating to be carried out well below the melting point of Ca (842 °C), a temperature at which it is quite volatile and will degrade most crucible materials. All the Ca/M/Zn phases were obtained from the Ca/Zn flux as brittle, gold-tinged rounded blocks up to

Table 6
Atomic positions for $Ca_6Pt_{2.34}Zn_{5.66}$

Atom	Wyckoff site	x	y	z	Occ.	U_{eq}
Pt1/Zn1	4*e*	1/4	0.58568(3)	0.18499(4)	0.714(6)/0.286(6)	0.0112(2)
Pt2/Zn2	2*a*	1/4	1/4	0.43643(5)	0.909(7)/0.091(7)	0.0108(2)
Zn3	4*e*	1/4	0.00485(9)	0.7486(1)	1	0.0182(3)
Zn4	2*b*	1/4	3/4	0.0672(2)	1	0.0129(4)
Zn5	4*e*	1/4	0.08636(8)	0.3178(1)	1	0.0117(3)
Ca1	4*e*	1/4	0.1007(2)	0.0227(2)	1	0.0142(4)
Ca2	4*e*	1/4	0.6127(2)	0.4687(2)	1	0.0131(4)
Ca3	2*b*	1/4	3/4	0.7548(2)	1	0.0127(6)
Ca4	2*a*	1/4	1/4	0.7328(3)	1	0.0143(6)

U_{eq} is defined as one-third of the trace of the orthogonalized U_{ij} tensor.

1 mm in diameter. It is possible that the crystals were etched as the flux was being dissolved, resulting in the loss of visible external faceting; crystals isolated via centrifugation appear to be larger and better formed. The materials are stable in air for at least a month, but are dissolved in acid solutions and degrade slowly in water. The stainless-steel crucibles appeared to be inert to the reaction mixtures studied in this work; no iron incorporation was indicated in the elemental analysis, and no magnetic secondary phases were apparent when the products were probed with a magnet.

3.1. $CaNi_2Zn_3$

This phase forms as the minority product (approximately 15% of the isolated solid) in syntheses with a 6:2:1 Ca:Zn:Ni ratio. Other phases found in the products include $Ca_{21}Ni_2Zn_{36}$ (60% of the isolated product; vide infra), $CaNi_2$ (5%), $CaZn_2$ (15%), and $CaZn_5$ (5%); it is presumed that any more calcium-rich phases that might form in the synthesis are degraded during the etching of the flux. The $CaNi_2Zn_3$ structure is related to the hexagonal $CaCu_5$ structure type observed for both $CaZn_5$ and $CaNi_5$ ($a = 4.9516$ Å, c = 3.9373Å and $a = 5.405$Å, $c = 4.183$Å, respectively) [8]. However, ordering of nickel and zinc atoms on the transition metal sites produces a superstructure ($a^* = \sqrt{3}a$ and $c^* = c$) although the space group type remains the same (*P6/mmm*). The resulting unit cell parameters ($a^* = 8.9814(5)$Å, $c^* = 4.0665(5)$Å) fall in the range expected for a $CaNi_xZn_{5-x}$ phase.

This ordered superstructure variant of the $CaCu_5$ type—the YCo_3Ga_2 structure type—is found in other phases such as $GdNi_3Ga_2$ and $RENi_3Al_2$ (RE = late rare-earth metal) [9]. Formation of the YCo_3Ga_2 form vs. the $CaCu_5$ form of a RET_xM_{5-x} compound appears to be dependent on composition ($2<x<3$) and temperature. In several reported cases, inter-conversion between the two structure types is observed when annealing is carried out, indicating the $CaCu_5$ form is the high temperature structure type and the YCo_3Ga_2 variant is the low temperature structure type [10]. The ordering in $CaNi_2Zn_3$ results in the preferential location of nickel atoms on sites closest to the electropositive calcium atoms, as would be expected from the higher electronegativity of nickel compared to zinc. As shown in Fig. 1, the Ca1 site is in a cylindrical environment with hexagonal symmetry, featuring 2.8310(9)Å bonds to six surrounding Ni atoms and 3.3245(6)Å distances to 12 nearest zinc atoms. The short Ca1–Ni bonds are surprising, but they are similar to those observed in $CaNi_2Si$ (2.862 Å) and $Ca_3Ni_3Si_2$ (2.837 Å, 2.852 Å) [11]. The Ca2 site of $CaNi_2Zn_3$ has lower symmetry compared to the Ca1 environment (−6m2 vs. 6/mmm site symmetry), but again features Ca–Ni distances (3.111(2)Å) that are shorter than the Ca–Zn distances (3.1912(5)Å). The nickel–zinc bonds fall in a very small range of 2.482–2.484 Å; zinc–zinc bonds are longer, ranging from 2.63 to 2.76 Å.

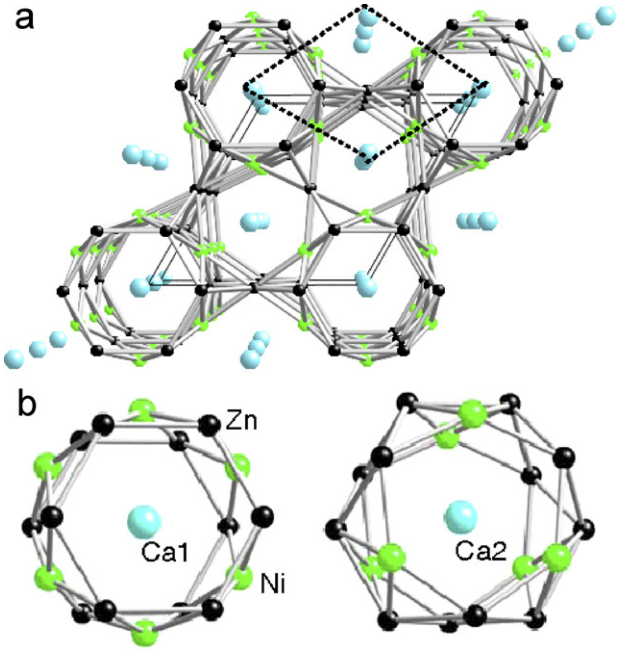

Fig. 1. (a) The $CaNi_2Zn_3$ structure type; the $CaCu_5$ substructure is indicated by a dashed unit cell. (b) The coordination environments of the two calcium sites in this structure.

Because of the similarity in atomic number, Ni and Zn sites are difficult to distinguish in the X-ray structure solution. However, the formation of the YCo_3Ga_2 type supercell, and the distinct difference in the bond lengths to

the Ni site compared to those to the Zn sites, support the idea that the $CaNi_2Zn_3$ compound is ordered. The occupancies of all five sites were allowed to vary in the last cycles of the refinement, but none of them varied significantly from one. Nevertheless, the possibility of Ni/Zn mixing on the non-calcium sites—producing a $CaNi_xZn_{5-x}$ stoichiometric range—cannot be ruled out. Because this is a minority product in the flux reactions and could not be obtained through stoichiometric reaction, powder diffraction analysis of unit cell size was not possible. It should be noted that zinc doping of the $CaNi_5$ phase to modify its hydrogen absorption capabilities has been previously investigated. Ball milling and annealing were used to synthesize $CaNi_{4.7}Zn_{0.3}$. The unit cell parameters increased as expected ($a = 5.0165$ Å, $c = 3.9545$ Å), but no supercell formation or preferred siting was reported at this level of zinc substitution [12].

3.2. $Ca_{21}Ni_2Zn_{36}$

This phase forms as the majority product in syntheses with a 6:2:1 Ca:Zn:Ni ratio. This is a possibly new structure that demonstrates the icosagenic character of zinc. Other intermetallic structures containing zinc icosahedra centered with a transition metal include δ-Co_2Zn_{15}, RT_2Zn_{20} (T = Fe, Ru, Co, Rh, Ni), and $Zn_{1-x}Pd_x$ [13]. In $Ca_{21}Ni_2Zn_{36}$, nickel-centered icosahedra (involving Ni1, Zn1, and Zn2; Ni–Zn bond lengths 2.539(1) and 2.592(1)Å; see Table 4) are linked together by the remaining zinc site (Zn3) to form a cubic unit cell shown in Fig. 2. The Zn–Zn bond lengths range between 2.63 and 2.75 Å, similar to those in $CaNi_2Zn_3$, with two exceptions. There is a shorter 2.535(3)Å Zn2–Zn2 bond linking together neighboring icosahedra; and the non-icosahedral Zn3 sites are linked to each other through a much longer bond of 2.896(2)Å to form triangles.

The $Ca_{21}Ni_2Zn_{36}$ structure can be viewed as a zinc network defining icosahedral holes filled with Ni atoms and larger sites filled with Ca atoms, but a more useful view is to consider the structure of the calcium network. This is a calcium-rich structure—three of the sites (Ca1, Ca2, and Ca3) are within a distance of 3.4–3.5 Å to each other; the fourth Ca site (Ca4) is considerably further away from other Ca atoms (over 4 Å) and is not considered a part of the calcium network. Linking together three of the calcium sites of $Ca_{21}Ni_2Zn_{36}$ results in a clathrate II type substructure (space group *Fd*–3*m* (#227)). This makes $Ca_{21}Ni_2Zn_{36}$ a part of the family of cubic compounds which have a clathrate II arrangement of alkali metal and/or alkaline earth metals surrounding a variety of anionic clusters. This is the first member of this class to have a zinc-rich stoichiometry. Previous examples of this family contain a preponderance of group 13 elements and include $K_{17}In_{41}$, $K_{39}In_{80}$, $Na_{22}Ga_{39}$, $Na_{35}Cd_{24}Ga_{56}$, $K_{14}Na_{20}In_{91.818}$ $Li_{13.182}$ and $Mg_{35}Cu_{24}Ga_{53}$ [14,15]. In these structures, linking the electropositive metals together will form the pentagonal

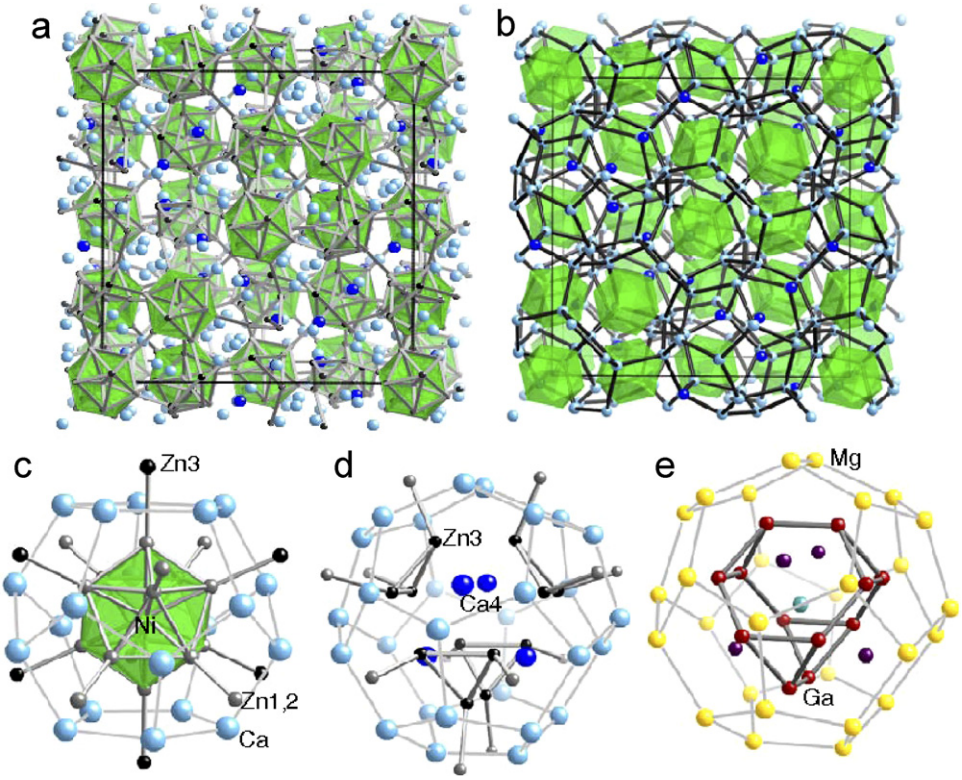

Fig. 2. The $Ca_{21}Ni_2Zn_{36}$ structure type: (a) view highlighting the linkages between the nickel centered icosahedra and additional zinc sites; calcium atoms are shown as non-bonded spheres, (b) view highlighting the clathrate II framework produced by connecting 3 of the calcium sites, (c) the pentagonal dodecahedron of calcium sites, encapsulating the $Ni@Zn_{12}$ icosahedron, (d) the hexakaidecahedron of calcium sites, encapsulating the triangles of Zn3 atoms and the Ca4 site and (e) a comparison to the contents of the Mg_{26} hexakaidecahedron of $Mg_{35}Cu_{24}Ga_{53}$.

dodecahedra (a 20 atom polyhedron, A_{20}) and hexakaidecahedra (a 28 atom polyhedron, A_{28}) of the clathrate II structure. The Ni@Zn_{12} icosahedra of $Ca_{21}Ni_2Zn_{36}$ are encased in the pentagonal dodecahedra of calcium atoms. The larger tetrahedrally symmetric hexakaidecahedra formed by Ca1, Ca2, and Ca3 atoms contain the Zn3 and Ca4 sites. As shown in Fig. 2d, the four hexagonal windows of this polyhedron are adjacent to the four Ca4 atoms. Each of the pentagonal windows is capped by a Zn3 site; these zinc atoms are close enough to each other to form weak Zn3–Zn3 bonds, resulting in triangles.

The $Ca_{21}Ni_2Zn_{36}$ structure bears a strong resemblance to that of $Mg_{35}Cu_{24}Ga_{53}$—comprised of a Mg clathrate II network surrounding linked anionic Cu/Ga clusters—with a number of small differences.[15] The nickel-centered Ni@Zn_{12} icosahedra in $Ca_{21}Ni_2Zn_{36}$ are paralleled by empty Cu_6Ga_6 icosahedra in the gallide phase. Conversely, the cluster within the A_{28} hexakaidecahedra is centered by a Mg atom in $Mg_{35}Cu_{24}Ga_{53}$ and it is empty in the compound studied in this work (Figs. 2d and 2e). The Mg@Ga_{16} cluster is described as an icosioctahedron, generated by linking together 12 Ga atoms (four triangles of Ga connected to form a truncated tetrahedron) and capping the four hexagonal faces with additional Ga sites. This parallels the four triangles of Zn3 seen in $Ca_{21}Ni_2Zn_{36}$, but these triangles are not close enough to form bonds between them (Zn3–Zn3 bonds within triangles are 2.896 Å; between triangles, the Zn–Zn distance is 3.324 Å). The Ga sites capping the hexagonal faces in the Mg@Ga_{16} cluster are replaced by Ca4 atoms in the structure studied here.

As in the case of $CaNi_2Zn_3$, mixing of Ni/Zn on the non-calcium sites of the $Ca_{21}Ni_2Zn_{36}$ structure cannot be ruled out. Nickel and zinc sites were assigned based on bond lengths and comparison to features of known structures (such as the Ni@Zn_{12} icosahedron in the TNi_2Zn_{20} phases). Again, the Ni–Zn bond lengths are shorter than the Zn–Zn bond lengths for the most part. A number of different crystals of the $Ca_{21}Ni_2Zn_{36}$ phase, synthesized in different reactions with different reactant ratios, were screened on the single-crystal diffractometer; the unit cell parameter did not vary greatly ($a = 21.505(8)$–$21.513(9)$Å). This compound could not be synthesized by stoichiometric combination of the elements, but powder diffraction of flux reaction products indicated a unit cell of $a = 21.53(2)$Å, only slightly larger than those shown in the single-crystal data. This small observed range supports the idea that this phase is most likely highly ordered.

3.3. $CaPd_{0.85}Zn_{1.15}$

The only ternary phase resulting from the combination of Ca, Pd, and Zn is the roughly 1:1:1 stoichiometry compound with the orthorhombic TiNiSi structure. This is a common structure type for intermetallics containing equimolar amounts of an electropositive element, a heavy late transition metal, and a main group element; analogs include HoIrSi, CaAuIn, and EuPtIn [16,17]. The Zn atoms in CaPdZn are tetrahedrally coordinated by four Pd

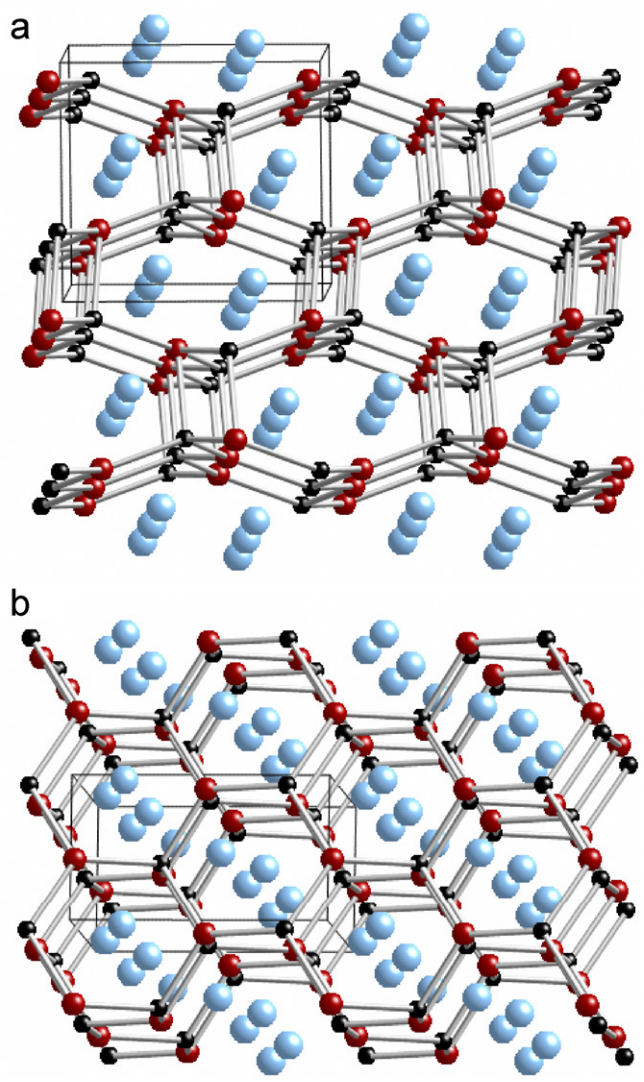

Fig. 3. The CaPdZn structure (TiNiSi structure type). Large blue spheres are Ca; small red spheres are Pd; small black spheres are Zn atoms: (a) view down the *b*-axis and (b) view down the *a*-axis, highlighting the relationship to the AlB_2 structure type.

atoms, with Zn–Pd bonds in the 2.6–2.7 Å range. The Pd atoms are also 4 coordinate, but in a less symmetric fashion. This can be considered a distortion of the hexagonal AlB_2 parent structure, a relationship that becomes evident upon viewing the structure down the *a*-axis (see Fig. 3) [18]. This structure type does allow for some solid solution, and Pd/Zn mixing is observed on the Pd site. An attempt to synthesize this compound from a 1:1:1 ratio of elements proved successful, yielding a poorly crystalline phase with orthorhombic unit cell parameters of $a = 7.136(7)$Å, $b = 4.421(5)$Å, $c = 7.755(9)$Å. The intensities of the peaks in the powder pattern match those calculated for CaPdZn using CrystalDiffract [19].

3.4. $Ca_6Pt_3Zn_5$

This ternary phase was obtained in low yield (30%, based on amount of Pt used), with $CaZn_2$ being the other

predominant phase isolated in the synthesis. This compound forms in an orthorhombic structure type (space group *Pmmn*) that is a new variant of the structure of W_3CoB_3 and $Sm_3Ir_2Si_2$ [11,17]. Both of these compounds have *Cmcm* symmetry, with unit cell parameters similar to $Ca_6Pt_3Zn_5$ (for $Sm_3Ir_2Si_2$, $a = 4.0969(2)$Å, $b = 10.5932(7)$Å; $c = 13.2753(8)$Å). The atomic locations are identical; the symmetry lowering is due to the variation in ordering of the atoms on the crystallographic sites in the unit cell. The puckered Pt/Zn sheets in Fig. 4b correspond to the CoB_3 sheets in W_3CoB_3 and the Ir_2Si_2 sheets in $Sm_3Ir_2Si_2$. Compared to the puckered Ir/Si sheet (shown in Fig. 4c), the pattern of site occupancy seen in $Ca_6Pt_3Zn_5$ results in loss of local symmetry elements such as mirror planes and inversion centers, causing a lowering of the overall space group symmetry from *Cmcm* to *Pmmn*.

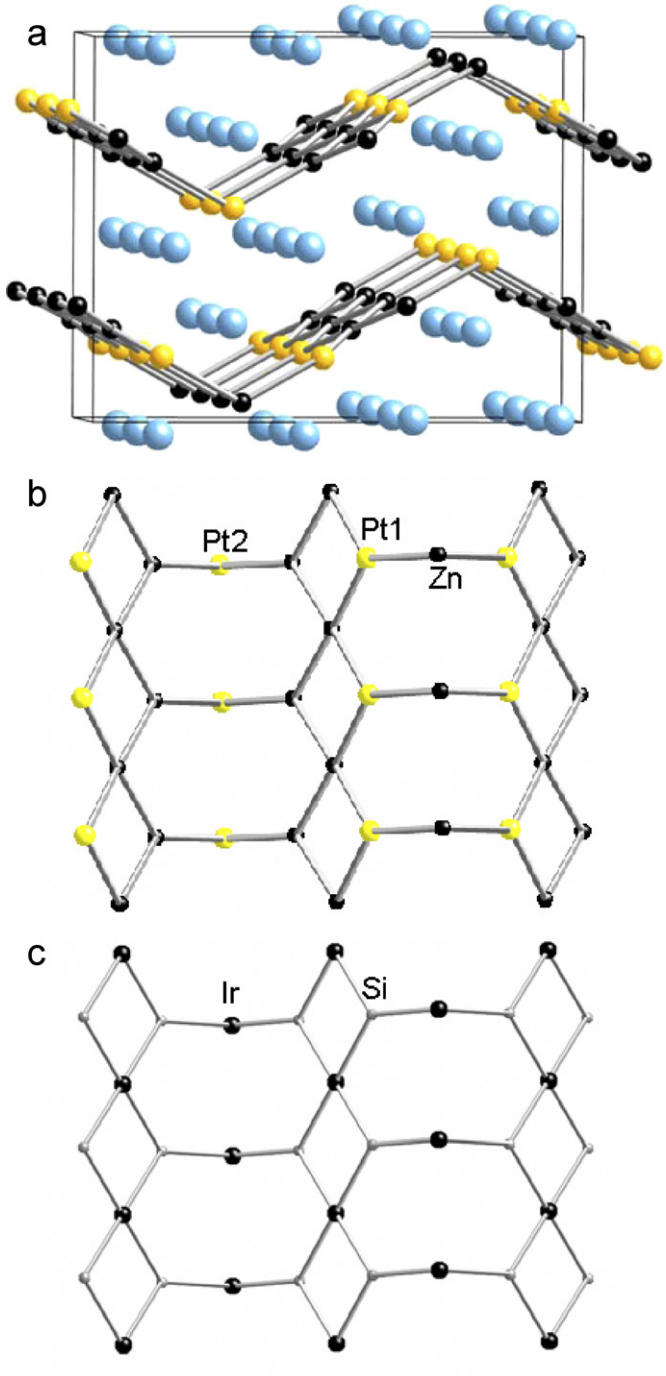

Fig. 4. The $Ca_6Pt_3Zn_5$ structure: (a) view down the *b*-axis, showing the puckered sheets formed by the Pt and Zn sites, (b) an individual sheet viewed down the *c*-axis, showing the distribution of Pt and Zn and (c) comparison to the higher symmetry Ir/Si puckered sheet of $Sm_3Ir_2Si_2$.

The late transition metals in $Sm_3Ir_2Si_2$ and W_3CoB_3 occupy the square planar site in the puckered layers of this structure; it is somewhat surprising that the platinum atoms in $Ca_6Pt_3Zn_5$ do not. Both of the platinum sites are partially occupied by zinc atoms (resulting in an actual stoichiometry of $Ca_6Pt_{2.34}Zn_{5.66}$), but there does not appear to be any evidence of platinum mixing into the square planar zinc site. The siting of platinum may be directed by promotion of short Pt–Ca distances; the Pt sites are within 3.0–3.2 Å of several calcium atoms. The zinc sites are further away from the calcium atoms on average. As in the case of $CaNi_2Zn_3$, the favorable interaction between the relatively electronegative transition metal atoms and the electropositive calcium atoms may stabilize the ordering of atoms in the structure. Band structure calculations are needed to further investigate this aspect of these phases.

4. Conclusion

Ca/Zn eutectic has proven to be a useful synthesis media for new intermetallic phases. Addition of group 10 transition metals to this flux results in the formation of new materials. Initial investigations into replacing Ni, Pd, and Pt with other transition metals (including Fe, Ru, Au, Ag, Mn) have proven unsuccessful thus far, yielding either $CaZn_2$ and unreacted transition metals, or known binary phases such as $CaAg_2$. Experiments are underway to explore additional reactants and to investigate the hydrogen storage and catalytic properties of the compounds synthesized in this work.

Acknowledgments

This research made use of the Scanning Electron Microscope facilities of MARTECH at Florida State University. Financial support from the NSF (Grant DMR-05-47791), the ACS Petroleum Research Fund, and an ORAU Ralph E. Powe Award is gratefully acknowledged. We thank J. Corbett, B. Li, and Q. Lin for useful discussions.

References

[1] Z. Fisk, J.P. Remeika, in: K.A. Gschneider, L. Eyring (Eds.), Handbook on the Physics and Chemistry of Rare Earths, Vol. 12, Elsevier Science, Amsterdam, 1989 (Chapter 81);
Z. Fisk, P.C. Canfield, Phil. Mag. 65 (1992) 1117–1123.
[2] M.G. Kanatzidis, R. Pöttgen, W. Jeitschko, Angew. Chem. Int. Ed. 44 (2005) 6996–7023.

[3] A. Zuttel, Naturwissenschaften 91 (2004) 157–172;
G. Sandrock, J. Alloy Compd. 293–295 (1999) 877–888.
[4] M. Morinaga, H. Yukawa, K. Nakatsuka, M. Takagi, J. Alloy Compd. 330–332 (2002) 20–24.
[5] SAINT, version 6.02a, Bruker AXS Inc., Madison, WI, 2000;
G.M. Sheldrick, SHELXTL NT/2000, version 6.1, Bruker AXS Inc., Madison, WI, 2000.
[6] L.M. Gelato, E. Parthe, J. Appl. Crystallogr. 20 (1987) 139–143.
[7] T.B. Massalski, H. Okamoto, Binary Alloy Phase Diagrams, second ed., ASM International, Materials Park, OH, 1990.
[8] P. Villars, L.D. Calvert, Pearson's Handbook—Crystallographic Data for Intermetallic Phases, ASM International, Materials Park, OH, 1998.
[9] M.A. Fremy, D. Gignoux, J.M. Moreau, D. Paccard, I. Paccard, J. Less-Common Met. 106 (1985) 251–255;
B. Šorgić, A. Drašner, Ž. Blažina, J. Alloy Compd. 356–357 (2003) 501–504;
Ž. Blažina, B. Šorgić, A. Drašner, J. Phys.: Condens. Matter 11 (1999) 3105–3114.
[10] H. Flandorfer, P. Rogl, K. Hiebl, E. Bauer, A. Lindbaum, E. Gratz, C. Godart, D. Gignoux, D. Schmitt, Phys. Rev. B 50 (1994) 15527–15541;
A. Drašner, Ž. Blažina, J. Alloy Compd. 359 (2003) 180–185.
[11] J. Glaser, Z. Anorg. Allg. Chem. 628 (2002) 1946–1950.
[12] G. Liang, J. Huot, R. Schulz, J. Alloy Compd. 321 (2001) 146–150.
[13] M. Böstrom, S. Lidin, J. Solid State Chem. 166 (2002) 53–57;
T. Nasch, W. Jeitschko, U.C. Rodewald, Z. Naturforsch. B 52 (1997) 1023–1030;
O. Gourdon, Z. Izaola, L. Elcoro, V. Petricek, G.J. Miller, Phil. Mag. 86 (2006) 419–425.
[14] B. Li, J.D. Corbett, J. Am. Chem. Soc. 127 (2005) 926–932;
G. Cordier, V. Müller, Z. Naturforsch. B. 49 (1994) 721;
B. Lin, J.D. Corbett, Inorg. Chem. 42 (2003) 8768;
M. Tillard-Charbonnel, N. Chouaibi, C. Belin, Mater. Res. Bull. 27 (1992) 1277.
[15] Q. Lin, J.D. Corbett, Inorg. Chem. 44 (2005) 512–518.
[16] D. Kußmann, R. Hoffmann, R. Pöttgen, Z. Anorg. Allg. Chem. 624 (1998) 1727–1735;
R. Pottgen, Z. Kristallog. 211 (1996) 884–890.
[17] R. Mishra, R. Hoffmann, R. Pöttgen, Z. Anorg. Allg. Chem. 627 (2001) 1787–1792.
[18] R.D. Hoffmann, R. Pöttgen, Z. Kristallogr. 216 (2001) 127–145.
[19] CrystalDiffract, version 1.0.2. M. Conley, D. Palmer, CrystalMaker Software Ltd., Oxfordshire, UK, 1994–2006.